Molecular Conformation and Nanomechanics of Self-Assembled Alkylsiloxane Monolayers

ARTICLE *in* LANGMUIR · JANUARY 1997

Impact Factor: 4.46 · DOI: 10.1021/la9605807

5 AUTHORS, INCLUDING:

Jung Y. Huang
Chiao Tung University
125 PUBLICATIONS **1,917** CITATIONS
SEE PROFILE

K. J. Song
Academia Sinica
26 PUBLICATIONS **514** CITATIONS
SEE PROFILE

Alexei Lagutchev
Purdue University
44 PUBLICATIONS **712** CITATIONS
SEE PROFILE

Pao-Keng Yang
Minghsin University of Science and Technology
26 PUBLICATIONS **183** CITATIONS
SEE PROFILE

Molecular Conformation and Nanomechanics of Self-Assembled Alkylsiloxane Monolayers

J. Y. Huang,* K. J. Song,† A. Lagoutchev,† P. K. Yang, and T. J. Chuang†

Institute of Electro-Optical Engineering, Chiao Tung University, Hsinchu, Taiwan, Republic of China, and Institute of Atomic and Molecular Sciences, Academia Sinica, P.O. Box 23-166, Taipei 10764, Taiwan, Republic of China

Received June 12, 1996⊗

We have studied the chain conformation and nanomechanical properties of pure alkylsiloxane monolayers and the mixed films with fluorine-containing species using scanning force microscopy (SFM) and infrared−visible sum-frequency generation spectroscopy (IV-SFG). Our IV-SFG spectra yield information about the chain ordering and surface density of specific species in the pure and mixed monolayers. A film formation process involving preferential adsorption of the fluorinated species from solution was observed. On the basis of the SFM measurements, the stiffness of alkylsiloxane monolayers under load was found to increase with the chain length, changes of chain conformation, and alkyl chain fluorination.

1. Introduction

Mechanical properties on a surface of solid materials crucially depend on the molecular composition and distribution. These surface properties can be modified with suitable surfactants.[1,2] Important applications can be realized with such surface modification techniques. However, to achieve this goal, sufficient understanding of the mechanism of the mechanical interactions between two solid objects and/or liquid−solid interfaces is needed.

Criteria for good boundary lubricants include strong adhesion to solid surfaces, significant reduction of the friction between two moving surfaces, and high stiffness under load. Recently, several developments in surface analytical techniques have allowed these tribological properties to be investigated at the nanometer scale.[3,4] Owing to its ideal tip-surface geometry, scanning force microscopy (SFM)[4] is suited for the study of the contact formation between two solid surfaces. Furthermore, SFM is highly versatile for application to various kinds of solid surfaces.

In many practical applications, solid objects are often immersed in liquids or located in ambient conditions. Very few surface analytical techniques can access such buried interfaces and yield information with sufficient surface sensitivity and molecular specificity. It has been realized that optical techniques can be applied to any interface accessible to light. Among the developments in optical techniques, infrared−visible sum-frequency generation spectroscopy (IV-SFG) is regarded as highly versatile with excellent surface sensitivity and molecular specificity.[5] Spectral information from IV-SFG is also crucial for a good understanding of the polar structure[6] of boundary lubricant layers.

We present here a study of the tribological properties of boundary lubrication layers by combining IV-SFG and SFM. Alkylsiloxane monolayers and their mixtures with fluorine-containing species are chosen for this investigation because these monolayers are good candidates for model studies of boundary lubrication. Insights gained from those model studies can be applied to more complex technological systems.

This paper is organized as follows: Section 2 briefly describes the techniques and sample preparation. Experimental results of SFM images, film stiffness, and IV-SFG spectra are presented in section 3. In section 4 discussion is given, and finally conclusions are drawn in section 5.

2. Experimental Section

2.1. Infrared−Visible Sum-Frequency Generation Spectroscopy. IV-SFG is a second-order nonlinear optical process in which two input beams, one at the infrared frequency (ω_1) and the other at the visible frequency (ω_2), interact and generate an output at the sum-frequency (ω_{sf}) in the visible spectrum of light. The sum-frequency signal is proportional to the absolute square of the effective surface susceptibility, $\chi^{(2)}{}_s$. In the case of a monolayer of adsorbates on a centrosymmetric substrate, the macroscopic nonlinear surface susceptibility of this layer can be related to the molecular nonlinear polarizability by a transformation from the molecular frame to the laboratory coordinates.[6] Pronounced resonance can be observed in $\chi^{(2)}{}_s$ if the incident infrared frequency is tuned across a vibrational mode of the adsorbed molecules in the interfacial layer. Thus, we can describe the sum-frequency intensity as

$$I(\omega_{sf}) \propto |\chi^{(2)}{}_s(\omega_{sf};\omega_1,\omega_2)|^2 = |\chi^{(2)}{}_{nr} + \sum_q \frac{A_q}{(\omega_1 - \omega_q + i\gamma_q)}|^2 \quad (1)$$

where $\chi^{(2)}{}_{nr}$ is the susceptibility from the nonresonant background and A_q, ω_q, and γ_q denote the resonant amplitude, frequency, and damping constant of the qth normal mode. These parameters can be determined with the fit of the measured spectrum to eq 1.

An IV-SFG apparatus similar to the one sketched in earlier publications[5] has been set up in our lab. The laser system produces picosecond visible (0.532 μm, 17 ps) and tunable infrared pulses (~17 ps) at ~3.5 μm with a 7 cm^{-1} line width, generated from a $LiNbO_3$ optical parametric generator/amplifier producing about 100 μJ per pulse on the surface of a monolayer sample at 20 pulses per second. The visible and infrared beams were overlapped on the sample surface with beam diameters of ~600 and ~200 μm, respectively. We adopt a nearly collinear incident beam geometry with a beam separation angle of less than 10°.

* Author to whom correspondence should be addressed. E-mail: jyhuang@cc.nctu.edu.tw. Fax: 886-3-5716631. Telephone: 886-3-5731975.

† Academia Sinica.

⊗ Abstract published in *Advance ACS Abstracts,* December 15, 1996.

(1) Radmacher, M.; Tillmann, R. W.; Fritz, M.; Gaub, H. E. *Science* **1992**, *257*, 1900−1905.

(2) Overney, R.; Meyer, E. *MRS Bull.* **1993**, *May 1*, 26−34.

(3) Israelachvili, J. N.; Adams, G. E. *J. Colloid Interface Sci.* **1973**, *44*, 975.

(4) Sarid, D. *Atomic Force Microscopy*; Oxford University Press: Oxford, 1991.

(5) Huang, J. Y.; Shen, Y. R. In *Laser Spectroscopy and Photochemistry on Metal Surfaces*; Dai, H. L., Ho, W., Eds.; World Scientific: Singapore, 1995; Adv. Ser. Phys. Chem. Vol. 5, Chapter 1.

(6) Shen, Y. R. *Annu. Rev. Mater. Sci.* **1989**, *16*, 69.

S0743-7463(96)00580-X CCC: $14.00

This angle makes the quadrupole contribution from substrate negligible while this angle is still large enough for an effective separation of the output sum-frequency ($\omega_{sf} = \omega_1 + \omega_2$) from the second-harmonic signal ($\omega_{sh} = 2\omega_2$).[5]

The tunable infrared source was calibrated to within 2 cm^{-1} with a polystyrene film. All sum-frequency spectra were recorded by a gated detection technique. Spatial filtering and a combination of a holographic filter and a monochromator were employed to help discriminate background noise arising from laser scattering or fluorescence and improve the signal-to-background ratio.

2.2. Scanning Force Microscopy. In SFM, a microfabricated cantilever with an integrated tip scans in close proximity to a material surface. The surface normal force can result in a vertical bending (z-axis) at the free end of the anchored cantilever.[7] As the tip scans along the perpendicular direction (x-axis) to the long axis of the cantilever beam, the friction force induces a torsional motion of the cantilever. A reflected laser beam from the backside of the cantilever is employed to monitor these cantilever motions. Since both of the cantilever motions are perpendicular to each other, keeping the normal force experienced by the tip constant, simultaneous image acquisition of the topography and friction force on the surface is allowed.

The deformation of the tip−sample system can be properly modeled by a spherical tip, which has a radius R, a Young's modulus E_1, and a Poisson ratio ν_1, and a planar sample surface with elastic properties described by E_2 and ν_2. Under the action of an external normal force F_z, the tip−sample system deforms to yield a relative motion Y of the system.[8−10] A local stiffness S can be deduced by approximating the normal force F_z to first order of Y:

$$F_z = F_{z0} + \left(\frac{\partial F_z}{\partial Y}\right)_{Y=0} Y = F_{z0} + SY \qquad (2)$$

where $F_{z0} = K_c z_0$ denotes the normal force experienced when the tip barely touches the sample surface without introducing a strain and K_c is the spring constant of the cantilever. The local stiffness S thus can be derived to be[1,11,12]

$$S \equiv \left(\frac{\partial F_z}{\partial Y}\right)_{Y=0} = \left(\frac{6E^{*2}RF_z}{\pi^2}\right)^{1/3} \qquad (3)$$

Here E^* is the effective Young's modulus of the tip−sample system, which can be expressed as

$$\frac{1}{E^*} = \frac{(1-\nu_1^2)}{E_1} + \frac{(1-\nu_2^2)}{E_2} \qquad (4)$$

We can determine the effective Young's modulus at position $\vec{r}$ on the sample surface by using a tip scanned over the sample surface. Experimentally this is performed with the z-position of the sample modulated by a small sinusoidal amplitude. Thus, from eq 3 we note that

$$E^*(\vec{r}) = \left(\frac{\pi^2 S^3}{6RF_z(\vec{r})}\right)^{1/2} = \sqrt{\frac{\pi^2}{6R}}\sqrt{\frac{S^3}{F_{z0} + SY(\vec{r})}} = \sqrt{\frac{\pi^2 S^3}{6RF_{z0}}}\left(1 + \frac{S}{F_{z0}}Y\right)^{-1/2} \cong \sqrt{\frac{\pi^2 S^3}{6RF_{z0}}}\left(1 - \frac{S}{2F_{z0}}Y\right) \qquad (5)$$

The above equation provides a necessary connection of the variation in local Young's modulus with the modulating amplitude of the tip−sample system $Y(\vec{r})$ by[1]

$$\Delta E^*(\vec{r}) = -\frac{SE^*(z_0)}{2F_{z0}}Y(\vec{r}) \qquad (6)$$

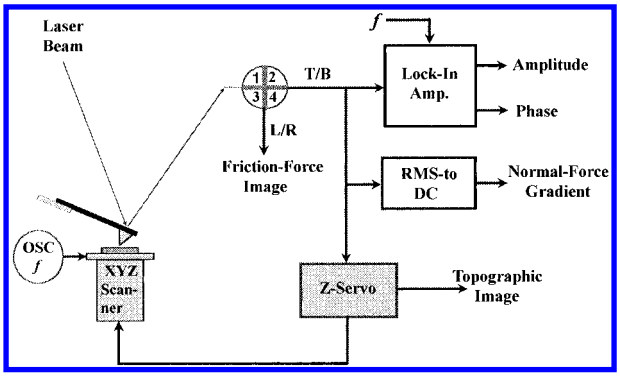

Figure 1. Schematic of a scanning force microscope which is able to simultaneously acquire images of topography, elasticity, viscosity, and normal force gradient of a thin-film sample. Here OSC f denotes an oscillator operated at frequency f which is used to modulate the z-position of the sample, RMS-to-DC is an electronic module which converts a modulated electrical signal into a direct-current value, and T/B and L/R represent the signal difference of the top−bottom and the left−right photon detectors.

Furthermore a phase shift observed in the modulating signal can be ascribed to originate from the viscosity of the sample.

A scanning force microscope used to acquire images of topography, friction force, and stiffness of self-assembled monolayers on a solid substrate is sketched in Figure 1. Our SFM measurements were performed with a standard 100 μm long, V-shaped, pyramidal-tipped silicon oxynitride cantilever which has a spring constant of about 0.4 nN/nm. A quadrant-segment position sensitive detector was used to monitor the direction of the reflected laser beam. The z-position of the samples was modulated at a frequency of f =12 kHz with an amplitude of 5 nm. This corresponds to a 2 nN force modulation. The modulating frequency is low enough for the mass effect of the cantilever to be negligible.[13,14] A signal-processing unit was employed to deduce the amplitude, phase, and root-mean-squared amplitude (rms-to-dc) from the input-modulated photosignal. The speed used to acquire force−distance curves was chosen to be 10 nm/s, which is sufficiently slow for achieving stabilized output from the signal-processing unit at each sampling point. A total of five different images of topography, friction force, elasticity, viscosity, and normal force gradient[15] can be acquired simultaneously. All SFM measurements were made at room temperature in air with a relative humidity less than 50%.

2.3. Calculations of Molecular Properties. The equilibrium geometry, the normal-mode frequencies, and the corresponding infrared absorption strengths[16] of $CF_3(CF_2)_5(CH_2)_2Si(OH)_3$ were calculated with the Amsterdam density functional package.[17] The calculations were carried out with a large core option. A sophisticated density functional, which includes a local density functional in the parametrization by Vosko *et al.*,[18] a nonlocal correlation correction by Perdew,[19] and a nonlocal exchange correction due to Becke,[20] has been used. The inner shell orbits were kept frozen in the calculations, and the valence electrons were described by a set of Slater-type orbitals of double-ζ parameters.[17]

The heat of formation for alkyltrichlorosilanes and their hydrolyzed products was calculated by modeling the conformation of the molecules in the gas phase with the semiempirical quantum-chemical program MOPAC 6 using the PM3 parametrization.[21] The keyword of PRECISION was used.

2.4. Sample Preparation. Octadecyltrichlorosilane (n-$C_{18}H_{37}SiCl_3$, C18H), n-octyltrichlorosilane (n-$C_8H_{17}SiCl_3$, C8H),

(7) Meyer, G.; Amer, N. W. *Appl. Phys. Lett.* **1990**, *57*, 2089.
(8) Johnson, K. L.; Kendal, K.; Roberts, A. D. *Proc. R. Soc. London* **1971**, *A324*, 301.
(9) Pethica, J. B.; Oliver, W. C. *Phys. Scr.* **1987**, *T19*, 61−66.
(10) Christenson, H. K. *Langmuir* **1996**, *12*, 1404.
(11) Overney, R. M.; Meyer, E.; Frommer, J.; Guntherodt, H.-J.; Fujihira, M.; Takano, H.; Gotoh, Y. *Langmuir* **1994**, *10*, 1281.
(12) Heuberger, M.; Dietler, G.; Schlapbach, L. *Nanotechnology* **1994**, *5*, 12.
(13) Wong, T. M. H.; Descouts, P. *J. Microsc.* **1995**, *178*, 7.
(14) Chen, G. Y.; Warmack, R. J.; Huang, A.; Thundat, T. *J. Appl. Phys.* **1995**, *78*, 1465.
(15) O'Shea, S. J.; Welland, M. E.; Pethica, J. B. *Chem. Phys. Lett.* **1994**, *223*, 336.
(16) Fan, L.; Ziegler, T. *J. Chem. Phys.* **1992**, *96*, 9005.
(17) Velde, Te; Baerends, E. J. *J. Comput. Phys.* **1992**, *99*, 84.
(18) Vosko, S. H.; Wilk, L.; Nusair, M. *Can. J. Phys.* **1980**, *58*, 1200.
(19) Perdew, J. P. *Phys. Rev.* **1986**, *B33*, 8822; **1986**, *B34*, 7406.
(20) Becke, A. D. *Phys. Rev. A* **1988**, *38*, 3098.
(21) Stewart, J. J. P. *Quantum Chemistry Program Exchange*; Indiana University, Bloomington, Indiana; Program 455, MOPAC Version 6.0.

and (tridecafluoro-1,1,2,2-tetrahydrooctyl)trichlorosilane (n-$C_6F_{13}CH_2CH_2SiCl_3$, C8F) were obtained from Petrach Systems, Inc, and were used as supplied. Polished fused silica glass plates and silicon wafers were employed as substrates. They were sufficiently cleaned by trichloroethane and acetone and then were subjected to ozone treatment to remove any residual hydrocarbon impurities. The surfaces were then immersed into piranha solution (1:3 H_2O_2/H_2SO_4)[22] followed by a rinse in deionized and distilled water. The substrates were then dried with filtered nitrogen.

Monolayers of the silanes were prepared by immersion into an 1 mM 4/1 n-hexadecane/CCl_4 solution.[23−25] Solutions of C8F tended to become cloudy after 20 min; therefore, C8F monolayer deposition is always completed within 10 min. The substrates were allowed to stand in the silanizing solution at 20 °C for various durations.[26] They were rinsed with chloroform and then dried with filtered nitrogen. The films were heated at 100 °C for 1 h. The surfaces obtained were highly hydrophobic with contact angles of ∼110° with water.

3. Experimental Results

3.1. Scanning Force Microscopy of Alkylsiloxane Monolayers. *Images of Alkylsiloxane Monolayers Self-Assembled on Silicon Substrates.* The images of the surface morphology of the C18H alkylsiloxane monolayer self-assembled on a silicon surface are presented in Figure 2. For comparison we first examine a clean silicon substrate, and its topographic image is shown in Figure 2a. Within an 1 μm × 1 μm scan range (only 0.5 μm × 0.5 μm is shown in Figure 2), the roughness of the bare silicon substrate was measured to be 0.7 Å. As a monolayer of C18H is deposited by dipping the substrate into a silanizing solution for 5 min, the film roughness increases to 5.1 ± 0.9 Å. Islandlike structures with an averaged size of 81 nm were clearly observed in Figure 2b. As the dipping time in C18H solution increases to 2 h, these surface features grow and merge to form a thicker film with improved film continuity. The topographic image of the film is shown in Figure 2c. Banga *et al.* observed a similar behavior in film formation with C18H.[27] Recently, Woodward and Schwartz[28] reported an *in situ* SFM study of the initial growth process of octadecylphosphonic acid on mica substrates. Those researchers discovered that the molecules aggregate into two-dimensional islands with a diameter of 10−20 nm while the substrate is still in solution.

The film morphology of C8H, C8F, and a mixed monolayer of C8H and C8F is similar to that observed on C18H. The roughness of the two pure monolayers was found to be 6.1 ± 0.2 Å for C8H and 4.1 ± 0.3 Å for C8F, while for the mixed monolayer a film roughness of 5.3 ± 0.5 Å was obtained. Our SFM study indicates that in the early film-assembling stage molecular species with longer chain length or a partially fluorinated chain lead to a smaller film roughness.

Film Stiffness of Alkylsiloxane Monolayers. More qualitative results of the nanomechanical properties of alkylsiloxane monolayers can be further deduced from force−distance measurements. The normal force, which is reflected in the cantilever deflection, is monitored as the tip moves toward and withdraws from a C18H-covered silicon substrate. The resulting force−distance curves are presented in Figure 3a with the solid line for tip-approaching and the dashed line for tip-retraction. Using our SFM setup, the force gradient can be measured simultaneously. We present these film stiffness curves in Figure 3b. With a known value of the cantilever's spring constant, the normal force applied on the film can be estimated, and the film stiffness as a function of loading force is shown in Figure 3c. It can be seen that the stiffness of the C18H monolayer has a fairly constant value as the load varies from 0 to 200 nN. Note that, with a 20 nm

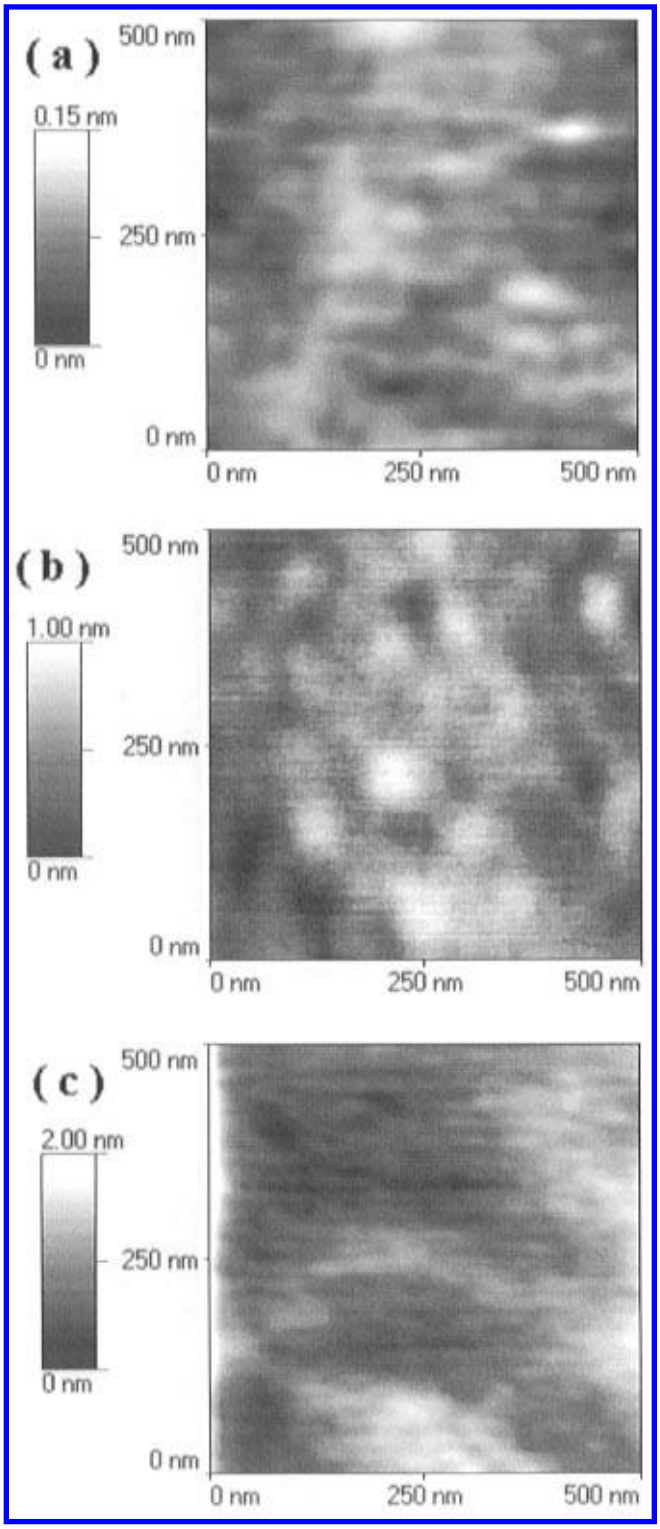

Figure 2. Topographic images of (a) a bare silicon substrate and (b and c) self-assembled $C_{18}H_{37}SiCl_3$ monolayers on silicon substrates. The films were prepared by dipping a substrate into 1 mM silanizing hexadecane for (b) 5 min and (c) 2 h.

(22) Green, J.-B. D.; McDermott, M. T.; Porter, M. D.; Spierko, L. M. *J. Phys. Chem.* **1995**, *99*, 10960.
(23) Le Grange, J. D.; Markham, J. L.; Kurkjian, C. R. *Langmuir* **1993**, *9*, 1749.
(24) Sagiv, J. *J. Am. Chem. Soc.* **1980**, *102*, 92.
(25) Ulman, A. *An Introduction to Ultrathin Organic Films from Langmuir−Blodgett to Self-Assembly*; Academic Press: San Diego, CA, 1991.
(26) Bierbaum, K.; Grunze, M.; Baski, A. A.; Chi, L. F.; Schrepp, W.; Fuchs, H. *Langmuir* **1995**, *11*, 2143.
(27) Banga, R.; Yarwood, J.; Morgan, A. M.; Evans, B.; Kells, J. *Langmuir* **1995**, *11*, 4393.
(28) Woodward, J. T.; Schwartz, D. K. *J. Am. Chem. Soc.* **1996**, *118*, 7861.

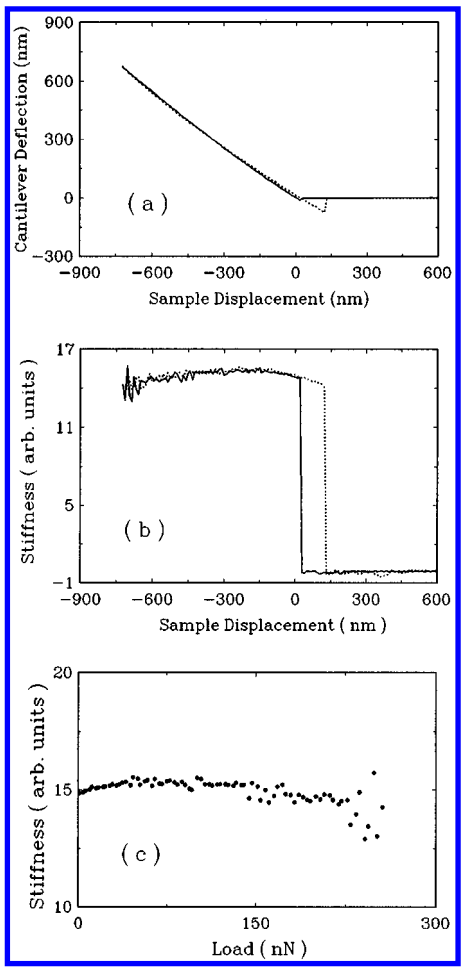

Figure 3. (a) Normal force and (b) normal force gradient between a SFM tip and a monolayer of C18H-covered silicon substrate plotted as functions of sample displacement. The solid curves are recorded with tip-approaching, while the dashed curves are for tip-retraction. (c) The force gradient during tip-approaching is replotted as a function of the loading force applied on the film.

radius tip pressed against a film, a 150 nN load readily generates a pressure as high as 120 MPa on the film.

Different behavior in the film stiffness from that observed with C18H was detected on alkylsiloxane monolayers with shorter or fluorinated alkyl chains. This can be clearly seen in Figure 4, where the measured curves of the film stiffness of C18H, C8H, C8F, and a mixed C8H−C8F monolayer under varying loads are shown. Note that the mixed monolayer, which was prepared by dipping a silicon substrate into a 1 mM solution with a mole fraction of 90% C8H and 10% C8F, has a surface concentration ratio of C8H/C8F = 2/1. These nanomechanical properties were measured with the same SFM tip; thus, the film stiffness indicated along the *y*-axis can be compared directly. It is found that the film stiffness of C8H linearly increases with loading force, while for C8F it first increases and then levels off as the load is higher than 150 nN. For the mixed monolayer, a saturated film stiffness appears at a loading force higher than 200 nN.

3.2. Infrared−Visible Sum-Frequency Generation Spectroscopy of Alkylsiloxane Monolayers. *Infrared−Visible Sum-Frequency Spectra of C18H and C8H.* It has been known that the friction between two moving surfaces can be significantly reduced by coating an alkylsiloxane layer on the surfaces. Recently, Salmeron *et al.*[29] observed a chain length dependence of the friction

(29) Xiao, X.; Hu, J.; Charych, D. H.; Salmeron, M. *Langmuir* **1996**, *12*, 235.

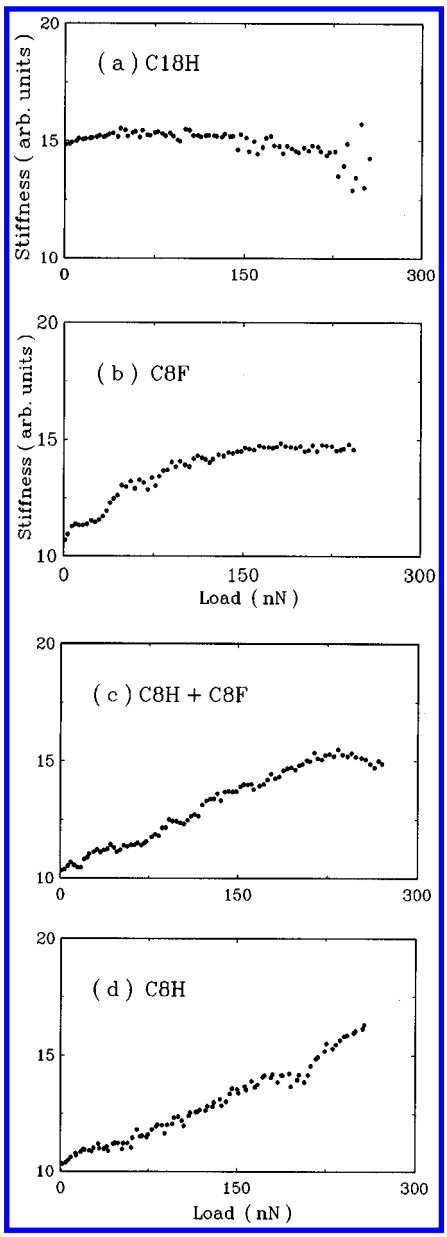

Figure 4. Normal force gradient recorded during tip-approaching plotted as a function of the loading force on a monolayer of (a) C18H, (b) C8F, (c) mixed C8H with C8F, and (d) C8H on a silicon substrate. The mixed monolayer shown in part c was prepared by dipping the substrate into a 1 mM hexadecane solution containing mixed alkyltrichlorosilane species with a mole fraction of C8F/C8H = 10/90, resulting in a surface concentration ratio of C8H/C8F = 2/1 for these two species.

reduction and had attributed the reduction to a high degree of lateral order within a layer with long alkyl chains. Our SFM measurements indicate that the C18H monolayer is stiffer than that of C8H under load and that fluorination of alkyl chains also can improve film stiffness.

To yield more insight into these mechanical properties at the molecular level, we apply IV-SFG for acquiring more information about the chain ordering. The IV-SFG results of C18H and C8H are given in Figure 5, where the dashed curve is the IV-SFG spectrum of C8H while the solid curve is for C18H. These spectra were taken with the input/output polarization being *s*-sum frequency, *s*-visible, and *p*-infrared (denoted hereafter as *ssp*). Three spectral features are clearly observed, all of which can be assigned to the CH stretches:[23] Those at 2850 and 2876 cm^{-1} arise from the symmetric (*s*) stretch of CH_2 and CH_3, respectively, and the one at 2935 cm^{-1} arises from the Fermi resonance (*f*-CH_3) between the *s*-CH_3 stretch and

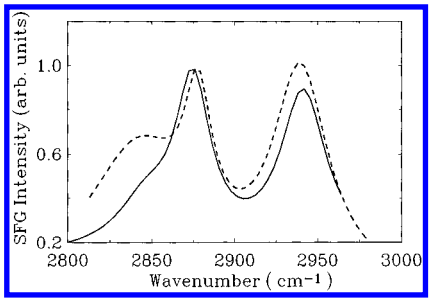

Figure 5. Infrared-visible sum-frequency spectrum of a monolayer of C18H (solid curve) and C8H (dashed curve) on a fused silica substrate. The spectra were taken with the input/output polarization being *s*-sum frequency, *s*-visible, and *p*-infrared, respectively.

the overtone of the CH_3 bending mode. The much weaker signal at 2850 cm^{-1} in C18H has previously been attributed to the near inversion symmetry of CH_2 along a straight alkyl chain.[30] The ratio of $A_q(s\text{-}CH_2)/A_q(s\text{-}CH_3)$ can be used to give a more quantitative comparison. For C18H, the ratio is measured to be 0.09 in comparison with 0.32 for the C8H monolayer. This result indicates that the octyl chain of the C8H monolayer has more cis−trans chain conformation defects than the octadecyl chain of C18H.[31]

IV-SFG Spectra of Mixed Films of C8H and C8F. We have tried to prepare a mixed monolayer of C8H and C8F on a silica substrate for modeling boundary lubricants with perfluoro additives. The *ssp* sum-frequency spectrum of a self-assembled monolayer, which was prepared by dipping a substrate into a 1 mM silanizing solution with a mixture of 50% mole fraction of C8H and 50% C8F, was found to be identical with that of a pure C8F monolayer. However, by investigating the monolayers prepared from sequentially dipping a substrate into two separate solutions containing pure alkyltrichlorosilane species, we found from the IV-SFG studies that alkylsilane molecules once adsorbed on substrates cannot be removed via a substitutive adsorption process. Therefore, we believe that an adsorption mechanism involving preferential adsorption of perfluoro alkylsilane species must be included to account for the observed film formation from mixed solution.

The competitive adsorption of C8F with the hydrocarbon species can be more clearly demonstrated with IV-SFG on mixed monolayers prepared from silanizing solutions with varying mole fractions of C8F. These spectra are presented in Figure 6. It is found that when the mole fraction of C8F in dipping solutions is higher than 20%, the sum-frequency spectrum of the resulting monolayer matches closely that of the pure C8F sample. The spectrum in Figure 6b shows that the sum-frequency activity of the $s\text{-}CH_2$ mode (∼2850 cm^{-1}) in the mixed monolayer has been effectively quenched with the coadsorption of a small quantity of the C8F species in the film. In addition, when Figure 6c is compared with Figure 6a and d, a significant intensity redistribution and frequency shift in the spectrum of the mixed monolayer were detected. Detailed analysis shows that the spectral peaks of both $s\text{-}CH_2$ and $s\text{-}CH_3$ in the mixed film are blue shifted from that of pure C8H, indicating that the structure of C8H in the mixed monolayer has been perturbed with the addition of perfluoro species at the molecular scale.

Figure 7 presents the sum-frequency resonant strength A_q/γ_q of various CH stretch modes as a function of the mole fraction of C8H in solution. All of the C−H stretch modes show a rapid change with the mole fraction of C8H varying from 0.8 to 1, which quantitatively supports that

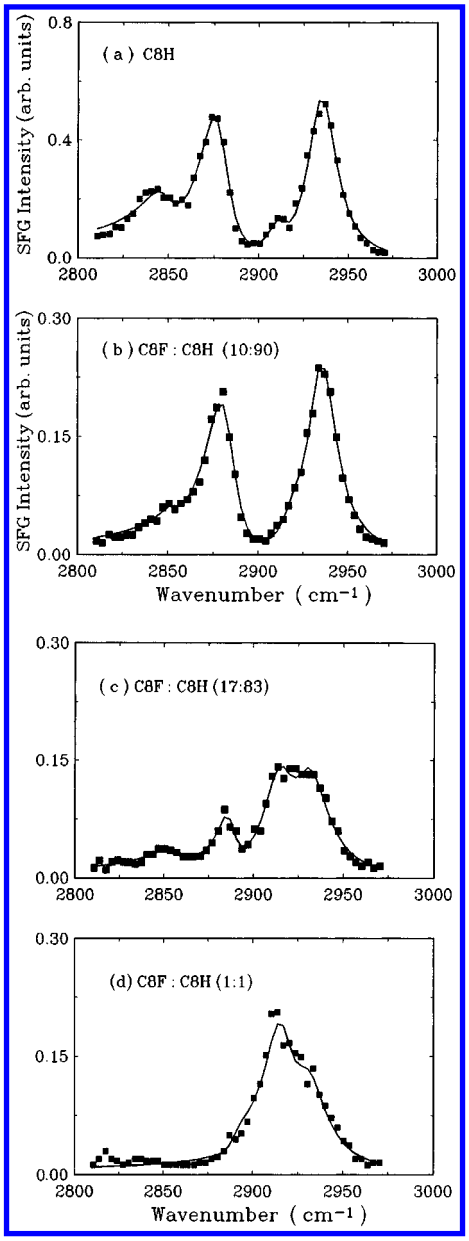

Figure 6. Infrared−visible sum-frequency spectra of mixed monolayers of C8F and C8H self-assembled on a fused silica glass surface. These mixed films were prepared by dipping a glass substrate into a 1 mM hexadecane solution containing mixed alkyltrichlorosilane species with a mole fraction of (a) C8F/C8H = 0/100, (b) C8F/C8H = 10/90, (c) C8F/C8H = 17/83, and (d) C8F/C8H = 50/50. The polarizations of the input infrared−visible and the output sum-frequency beams were taken to be *s*-, *s*-, and *p*-polarized, respectively.

the adsorption of the perfluoro species C8F from the solution phase onto the substrate is more effective than that of C8H.

4. Discussion

As has been pointed out in the previous section, film stiffness under load is a crucial parameter for boundary lubrication. Our SFM and IV-SFG results suggest that the longer chain length in an alkylsiloxane monolayer exhibits a higher chain ordering.

To explore the meaning embedded in Figure 4, we analyze the force−distance curves in more detail. By presenting the *z*-displacement of monolayer samples as Δ and the deflection of the cantilever as *D*, we then find that the force−distance curve can be expressed as[32]

$$D + Y = D + [K_c/S(\Delta)]D = \Delta \qquad (7)$$

(30) Guyot-Sionnest, P.; Hunt, J. H.; Shen, Y. R. *Phys. Rev. Lett.* **1987**, *59*, 1597.
(31) Touwslager, F. J.; Sondag, A. H. M. *Langmuir* **1994**, *10*, 1028.

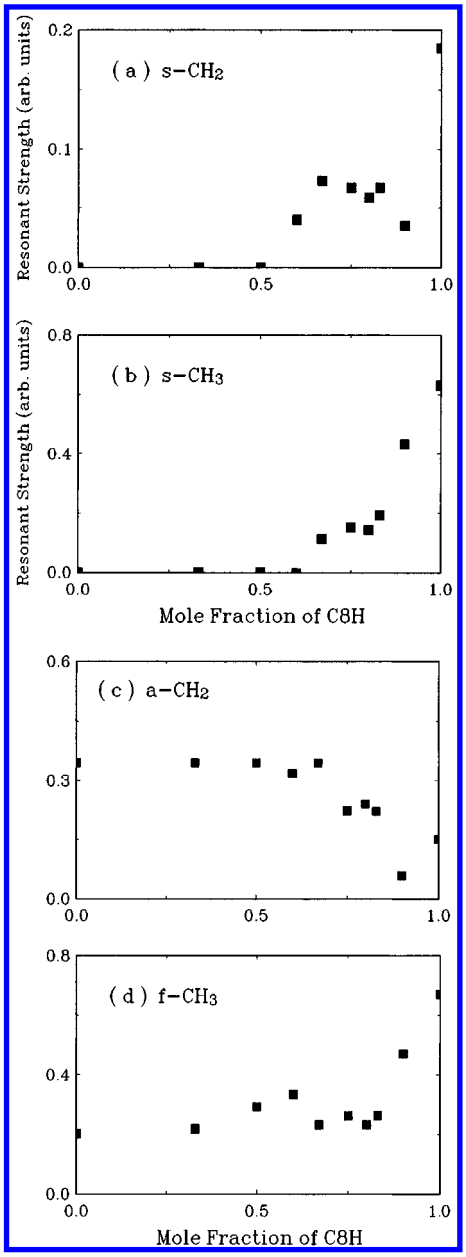

Figure 7. Resonant strength, A_q/γ_q, in the IV-SFG spectra of mixed films plotted as a function of the mole fraction of C8H in the dipping solution. (a) *s*-CH_2 (2850 cm^{-1}); (b) *s*-CH_2 (2880 cm^{-1}); (c) *a*-CH_2 (2915 cm^{-1}); (d) *f*-CH_3 (2935 cm^{-1}).

Assuming that film stiffness increases linearly with load by

$$S(\Delta) = (\partial F_z/\partial Y)_{Y=0} + a\Delta = S_0 + a\Delta \qquad (8)$$

then the force gradient−distance curve becomes

$$\frac{dD}{d\Delta} = \frac{1}{1 + \dfrac{K_c}{S(\Delta)}} + \frac{\dfrac{\Delta K_c\, dS}{S^2(\Delta) d\Delta}}{\left[1 + \dfrac{K_c}{S(\Delta)}\right]^2} \qquad (9)$$

We then find $dD/d\Delta \rightarrow 1$ at the rigid surface limit of $K_c \ll S$, while at the soft surface limit ($K_c \gg S$), $dD/d\Delta \cong (S + a)/K_c + (a/K_c)\Delta$. A transition regime where the force gradient switching from linear dependence on Δ to a constant can be met with the film stiffness under load being comparable to the spring constant of the cantilever. Since the SFM results shown in Figure 4 were obtained with the same SFM tip, we can then conclude that the film stiffness of these monolayers has an order of C18H > C8F > mixed film > C8H.

We have measured the surface coverage of monolayers of C18H, C8H, C8F, and a mixed C8H−C8F film using X-ray photoemission spectroscopy. Our results indicate that all these monolayer samples have a film packing similar to that of a compact alkylsiloxane monolayer. Thus we can rule out the possibility that the observed differences in the film stiffness may be caused by the variation in film packing.

Distortions in short chain molecules are in part due to thermal excitation. The stabilization energy per CH_2 group from van der Waals interaction is ~7 kJ/mol for molecules with C8H or longer alkyl chains. In light of the thermal energy at room temperature being ~2.5 kJ/mol, the 70 kJ/mol excess cohesion energy in the C18H monolayer compared with that of C8H can be the major cause of the higher in-plane chain ordering in C18H. As a result of the higher cohesion energy, monolayers with longer chains are therefore stiffer and more immune to the pressure exerted by the tip. Recently, using friction force microscopy, Salmeron *et al.*[29] concluded that the increased number of energy dissipation modes facilitated by the presence of molecular disorder dominates the frictional behavior in a short chain monolayer. Fluorination of alkyl chains enhances the chain rigidity and therefore may reduce the number of energy dissipation modes. Thus, monolayers with fluorinated species are expected to have an improved film stiffness over that of the corresponding pure hydrocarbon monolayer. This is supported by our SFM measurements.

In Figure 8a, the sum-frequency spectrum (open symbols) and the Fourier-transform infrared absorption spectrum (filled symbols) of a self-assembled C8F monolayer are shown. Assuming the two methylene groups of C8F in the trans configuration have identical bonding properties, the in-phase linear combination of *s*-CH_2 stretches should become strictly Raman active, while the π-phase-shifted combination is an infrared active mode. A similar situation holds for two *a*-CH_2 stretches. In view that a vibration mode must be both Raman and infrared active to have a nonvanishing sum-frequency intensity, it is thus surprising to find that only the *a*-CH_2 stretch (~2916 cm^{-1}) appears in the sum-frequency spectrum of C8F. To understand the underlying process that leads to this result, we optimize the equilibrium geometry of $CF_3(CF_2)_5(CH_2)_2Si(OH)_3$ and then calculate its normal mode frequencies and the corresponding infrared absorption strengths using the Amsterdam density functional package.[16,17] The fluorinated segment in the alkyl chain possesses a nonplanar helical geometry (see Figure 8b for the resulting molecular model). The calculated frequencies, normal mode coordinates, and infrared absorption strengths of some high-frequency normal modes are listed in Table 1. These C−H stretches are noted to far separate from other vibrational modes.

The two methylene groups in C8F turn out to have different bond lengths and bond polarizabilities owing to the difference in their chemical bonding environment. This provides necessary perturbation for frequency splitting and symmetry breaking in the formally pure Raman (*i.e.*, $d_+(0)$ and $d_-(0)$) and infrared active modes ($d_+(\pi)$ and $d_-(\pi)$). By defining $\Delta\omega_Q$ and r_Q as the frequency splitting and the ratio of the infrared absorption strengths of the symmetry-breaking modes, we then find from Table 1 that $\Delta\omega_Q$ and r_Q increase from $\Delta\omega_Q = 7$ cm^{-1} and $r_Q = 0.1$ for the CH_2 scissors motion to 12 cm^{-1} and 0.7 for the *s*-CH_2 stretch and then to 20 cm^{-1} and 1.01 for the *a*-CH_2 stretch.

(32) Aime, J. P.; Elkaakour, Z.; Odin, C.; Bouhacina, T.; Michel, D.; Curely, J.; Dautant, A. *J. Appl. Phys.* **1994**, *76*, 754.

Table 1. Calculated Vibration Frequencies, Infrared Absorption Strengths, and Normal Mode Coordinates of Some High Frequency Normal Modes of $CF_3(CF_2)_5(CH_2)_2Si(OH)_3$

ω_Q[a] (cm^{-1})	IR absorption strength	normal mode coordinates[b]	comment
1386	6.6	$\Delta\theta_1 + \Delta\theta_2$	CH_2 scissors motion (Raman active)
1379	65.3	$\Delta\theta_1 - \Delta\theta_2$	CH_2 scissors motion (infrared active)
2843	9.5	$\Delta r_1 + \Delta r_2 + \Delta r_3 + \Delta r_4$	$d_+(0)$, *s*-CH_2 stretches (Raman active)
2855	12.5	$\Delta r_1 + \Delta r_2 - \Delta r_3 - \Delta r_4$	$d_+(\pi)$, *s*-CH_2 stretches (infrared active)
2892	7.9	$\Delta r_1 - \Delta r_2 + \Delta r_3 - \Delta r_4$	$d_-(0)$, *a*-CH_2 stretches (Raman active)
2912	7.8	$\Delta r_1 - \Delta r_2 - \Delta r_3 + \Delta r_4$	$d_-(\pi)$, *a*-CH_2 stretches (infrared active)

[a] Frequencies were scaled with a multiplying factor of 0.96.[37] [b] Here $\Delta\theta_i$ represents the angular change during the scissors motion of the *i*th methylene group, and Δr_i denotes the bond length change along the C_i-H_i bond.

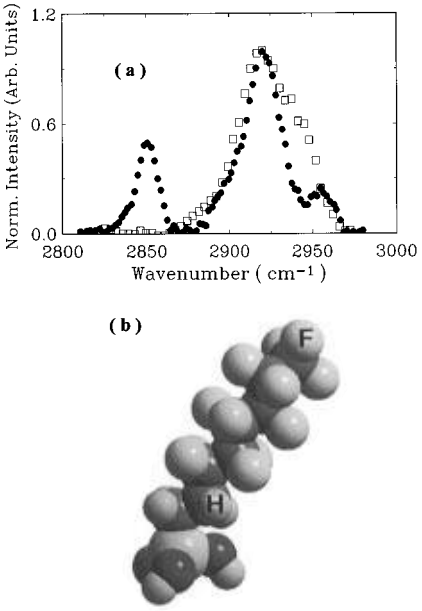

Figure 8. (a) Comparison of sum-frequency (open squares) and Fourier-transform infrared absorption (filled circles) spectra of a pure C8F monolayer. (b) Molecular model of $CF_3(CF_2)_5(CH_2)_2Si(OH)_3$ obtained from geometry optimization using the Amsterdam density functional package.

Note that the degree of symmetry breaking in the in-phase ($d_-(0)$) and π-phase-shifted ($d_-(\pi)$) combinations of *a*-CH_2 stretches increases to such a high level that the infrared absorption strength of $d_-(\pi)$ becomes even weaker than that for the formally pure Raman active mode $d_-(0)$. Owing to less symmetry breaking, the π-phase-shifted combination of two *s*-CH_2 stretches ($d_+(\pi)$) can yield a much weaker sum-frequency intensity than that for the *a*-CH_2 stretch.

Our sum-frequency measurements with self-assembled alkylsiloxane monolayers prepared from mixed silanizing solutions support a preferential adsorption process of the perfluoro species onto solid substrates. Thompson *et al.*[33] recently investigated the role of solvent on the silanization of glass with C18H and proposed a mechanism for the self-assembling process. This mechanism involved extraction of surface moisture into the bulk solvent, followed by C18H hydrolysis in the bulk solvent phase and then subsequent deposition on the solid surface. We have performed semiempirical PM-3 calculations[21] of the difference in the heat of formation for alkyltrichlorosilanes and their hydrolyzed products. It was found that the energy released in the C8F hydrolysis is larger than that of C8H by 21 kJ/mol; thus, it supports the notion that the preferential adsorption of C8F onto solid surfaces can be originated from the faster hydrolysis of $SiCl_3$ in perfluoro alkyl species than that of the hydrocarbon chain.

The dipping solution used in preparation of self-assembled alkyltrichlorosilane monolayers behaves like a lubricant in a mechanical system,[34] while the self-assembled alkylsiloxane monolayer serves as the boundary lubrication layer.[35] The preferential adsorption of perfluoro species onto solid surfaces from a solution as observed with IV-SFG spectroscopy indicates that when two solid objects start to contact by squeezing out the bulk lubrication layer, the perfluoro species readily adsorb on the bare region to provide the final protection. Thus, the results described in this paper provide an understanding basis for the common practice of adding perfluoro species into a lubricant to improve lubrication and reduce wear of solid objects.

5. Conclusions

The nanomechanics and chain conformation of several alkylsiloxane monolayers self-assembled onto solid substrates have been investigated with scanning force microscopy (SFM) and infrared−visible sum-frequency generation spectroscopy (IV-SFG). From the studies, the chain ordering and film stiffness of alkylsiloxane monolayers are found to increase with chain length and fluorination of the alkyl chains. The improvements in the chain ordering and film rigidity have been attributed to higher cohesion energy from interchain van der Waals interaction. A film formation process involving preferential adsorption of perfluoro species onto solid surfaces from solution is observed. This is supported by the fact that fluorination of the alkyl chains enhances the hydrolysis of trichlorosilane. Our studies with IV-SFG and SFM not only demonstrate the efficacy of the combined techniques for these important topics but also reveal the correlation of the nanomechanical properties of self-assembled films with the chemical structure[36] and chain ordering.

Acknowledgment. This work was supported by the National Science Council of the Republic of China under Grant Nos. NSC83-0208-M009-069 and NSC85-2113-M001-032.

LA9605807

(33) McGovern, M. E.; Kallury, K. M. R.; Thompson, M. *Langmuir* **1994**, *10*, 3607.

(34) Ouinn, T. F. J. *Physical Analysis for Tribology*; Cambridge University Press: Cambridge, U.K., 1991.

(35) Clechet, P.; Martelet, C.; Belin, M.; Zarrad, H.; Jaffrezic-Renault, N.; Fayeulle, S. *Sens. Actuators* **1994**, *A44*, 77. Ruhe, J.; Novotny, V. J.; Kanazawa, K. K.; Clarke, T.; Street, G. B. *Langmuir* **1993**, *9*, 2383.

(36) Liu, Y.; Evans, D. F.; Sung, Q.; Grainger, D. W. *Langmuir* **1996**, *12*, 1235.

(37) El-Azhary, A. A.; Suter, H. U. *J. Phys. Chem.* **1996**, *100*, 15056.